Adaptive kernels for multi-fiber reconstruction*

Angelos Barmpoutis[1], Bing Jian[2], and Baba C. Vemuri[1]

[1] CISE Department, University of Florida, Gainesville FL 32611, USA
[2] Siemens Healthcare, IKM CKS, Malvern, PA 19355, USA
abarmpou@cise.ufl.edu, bing.jian@siemens.com, vemuri@cise.ufl.edu

Abstract. In this paper we present a novel method for multi-fiber reconstruction given a diffusion-weighted MRI dataset. There are several existing methods that employ various spherical deconvolution kernels for achieving this task. However the kernels in all of the existing methods rely on certain assumptions regarding the properties of the underlying fibers, which introduce inaccuracies and unnatural limitations in them. Our model is a non trivial generalization of the spherical deconvolution model, which unlike the existing methods does not make use of a fix-shaped kernel. Instead, the shape of the kernel is estimated simultaneously with the rest of the unknown parameters by employing a general adaptive model that can theoretically approximate any spherical deconvolution kernel. The performance of our model is demonstrated using simulated and real diffusion-weighed MR datasets and compared quantitatively with several existing techniques in literature. The results obtained indicate that our model has superior performance that is close to the theoretic limit of the best possible achievable result.

1 Introduction

Many diffusion MR reconstruction methods are based on the Stejskal-Tanner equation $S = S_0 \exp(-bd)$ which describes the signal S observed in a diffusion MR image at a voxel scale, where b is the diffusion weighting factor depending on the strength as well as the effective time of diffusion, S_0 is the signal in the absence of any diffusion weighting, and d is called *apparent diffusion coefficient* (ADC) [1]. In the diffusion tensor imaging (DTI)[2], d is assumed to take a quadratic form $d = \mathbf{g}^T\mathbf{D}\mathbf{g}$, where $\mathbf{D}$ is a 3×3 positive definite matrix, and $\mathbf{g}$ is the diffusion gradient direction. However, the inability of DTI to deal with regions containing intra-voxel orientational heterogeneity has been widely reported in literature [3–6] making it a well-known and challenging problem.

To overcome the single fiber orientation limitation inherent with the unimodal quadratic functions, higher order models [3, 4, 7] have been proposed to model the diffusivity function. However, the flexibility brought by these methods

* This work was supported by NIH under Grants EB007082 and P41-RR16105. Authors thank Drs. Timothy M. Shepherd and Evren Özarslan for data acquisition. Implementation is available at http://www.cise.ufl.edu/research/cvgmi/Software.php

does not solve the problem that the peaks of the ADC profile do not necessarily yield the fiber orientations in the case of fiber crossings [8, 9].

The ensemble-average diffusion propagator P(r,t) can be computed using the q-space methods by exploiting the Fourier relation between the signal attenuation and the diffusion propagator. Diffusion spectrum imaging (DSI) [10] performs a discrete Fourier transform to obtain P(r,t), which requires a time-intensive Cartesian sampling in q-space and hence is impractical for routine clinical use. Instead of the Cartesian sampling, the Q-ball imaging (QBI) method takes measurements on a q-space ball and approximates the radial integral of the displacement probability distribution function by the spherical Funk-Radon transform [11]. In more recent studies, the analytic solution of QBI's Funk-Radon transform has been derived by using a spherical harmonic basis [12–14]. One problem with QBI is that the estimated diffusion ODF is modulated by a zeroth-order Bessel function that induces spectral broadening of the diffusion peaks. Another technique called the diffusion orientation transform (DOT) [8] computes the displacement probability profile at a fixed radius by expressing the Fourier transform in spherical coordinates and evaluating the radial part of the integral analytically. DOT assumes signals decay can be described by either a mono- or a multi-exponential model, the latter of which requires data acquisition over multiple concentric spheres, a time consuming proposition.

Another research direction in the multi-fiber reconstruction literature is to describe the signal attenuation by multi-compartment models beyond the mono-exponential Stejskal-Tanner equation. The approach in [6] assumes the signal in each voxel can be split into a weighted sum of contributions from different diffusion tensors individually. Various partial volume models have been studied in [15, 16] and were extended in [17, 18]. The model selection problem in these methods usually requires complicated solution techniques and computationally intensive simulations to infer the optimal model parameters properly.

To avoid the model-selection problem several spherical deconvolution techniques have been proposed in which the DW-MRI signal can be expressed as the convolution over the sphere of a fiber bundle response (also known as kernel function k) with a probability density function [19–22]. In this spherical deconvolution approach there is no limitation on the number of the estimated distinct fiber populations within a voxel. However, all of these methods employ a predefined fix-shaped function such as Gaussian [19, 21, 23], von Mises [22], Rigaut-type [20], each of which is treated as a spherical basis, whose shape parameters are chosen based on certain assumptions relating to the properties of the underlying fibers. Such assumptions introduce inaccuracies and unnatural limitations in the methods since in a real DW-MRI dataset the properties of the underlying fibers may vary spatially.

In this paper we present a novel mathematical model for multi-fiber reconstruction using an adaptive deconvolution kernel, whose shape is not fixed and is estimated simultaneously with the rest of the unknowns of the model. The adaptive kernel is defined as a spline over the space of magnetic gradient directions and the diffusion weighting factor b, which can theoretically approximate any

continuous function. We present extensive comparisons between the proposed method and other existing techniques demonstrating superior performance of our method. Furthermore we show that the results produced by the proposed model are close to the limit of the theoretically best possible result.

The main contribution of this paper is a novel mathematical model for multi-fiber reconstruction. To the best of our knowledge, it is the first method that employs an adaptively shaped spherical deconvolution kernel instead of a fixed one used by the existing techniques. Our model overcomes the limitations of the other methods and furthermore generalizes the spherical deconvolution framework, in which all the other existing methods can be expressed as special cases.

2 Mathematical model

The DW-MRI signal response can be modeled as the convolution of a kernel function k, which corresponds to a single fiber response, with a mixing density function f as expressed in the following equation

$$S(b, \mathbf{g})/S_0 = \int f(\mathbf{p}) k(b, \mathbf{g}|\mathbf{p}) d\mathbf{p} \tag{1}$$

where the kernel k is a parametric function with parameter vector $\mathbf{p}$, which is also the random variable of the density function f, and the integration is over the domain of $\mathbf{p}$. S_0 is the zero gradient image, and $\mathbf{g}$ and b are the magnetic gradient field direction and the b-value respectively. In [24], it has been shown that several existing multi-fiber reconstruction models can be expressed in the above generalized fiber convolution model.

Two possible choices for the kernel function are the multivariate Gaussian function $k(b, \mathbf{g}|\mathbf{D}) = e^{-b\mathbf{g}^T\mathbf{D}\mathbf{g}}$ [12, 19–21], and the von Mises-Fisher function over the sphere given by $k(b, \mathbf{g}|\mu) = \frac{\kappa}{4\pi sinh\kappa} e^{\kappa\mu^T\mathbf{g}}$ [22]. The integration space in the above examples is the space of 3×3 symmetric positive-definite matrices $\mathbf{D}$ and the space of 3-dimensional unit vectors μ respectively. The kernel functions as well as the mixing densities that correspond to several existing multi-fiber reconstruction models are reported and compared in [24].

Due to the spherical nature of the diffusion-weighted acquisition process, the mixing density function f can be parametrized using a discrete hemispherical lattice as follows

$$f(\mathbf{p}) = \sum_{j=1}^{N} w_j \phi(\mathbf{p}|\mathbf{v}_j) \tag{2}$$

where $\mathbf{v}_1 \ldots \mathbf{v}_N$ is a set of unit vectors uniformly distributed on the hemisphere, and $\phi(\mathbf{p}|\mathbf{v}_j)$ is a mixing density function that is treated here as a basis function weighted by the unknown mixing weights w_j. By substituting Eq. 2 into Eq. 1 and convolving these basis functions with the kernel over the space of the kernel's parameters as follows

$$\int \sum_{j=1}^{N} w_j \phi(\mathbf{p}|\mathbf{v}_j) k(b, \mathbf{g}|\mathbf{p}) d\mathbf{p} = \sum_{j=1}^{N} w_j K(b, \mathbf{g}|\mathbf{v}_j) \tag{3}$$

we obtain a continuous function $K(b, \mathbf{g}|\mathbf{v}_j) = \int \phi(\mathbf{p}|\mathbf{v}_j)k(b, \mathbf{g}|\mathbf{p})d\mathbf{p}$. In several cases, this function can be computed analytically [20, 22] and corresponds to a multi-fiber reconstruction kernel K, employed in the following mixture model

$$S(b, \mathbf{g})/S_0 = \sum_{j=1}^{N} w_j K(b, \mathbf{g}|\mathbf{v}_j) \tag{4}$$

Different choices of $k(b, \mathbf{g}|\mathbf{p})$ in Eq.(1) and of $\phi(\mathbf{p}|\mathbf{v}_j)$ in Eq.(2) result in differently shaped kernel $K(b, \mathbf{g}|\mathbf{v}_j)$ in Eq.(4). Thus it is entirely possible for some kernels to be better suited to a particular data set than others in terms of reconstruction accuracy.

In all of the existing methods, the shape of the kernel K is assumed to be fixed, which is an unnecessary constraint and adds an unnatural restriction to the computed fiber reconstructions. For example the shape of the Rigaut-type kernel $K(b, \mathbf{g}|, \mathbf{T}_j) = (1 + (b\mathbf{g}^T\mathbf{T}_j\mathbf{g})/p)^{-p}$ derived in [20] is fixed by using certain predefined value of p as well as eigenvalues in the tensor $\mathbf{T}_j$, the diffusion basis kernel $K(b, \mathbf{g}|\mathbf{T}_j) = exp(-b\mathbf{g}^T\mathbf{T}_j\mathbf{g})$ in [19, 21] is also fixed by predefining the eigenvalues of the tensor, and the shape of the model employed in [22] is fixed by choosing a value for the parameter κ.

In this paper, we do not make any such assumptions instead, we develop a general adaptively shaped kernel, whose shape is simultaneously estimated with the mixing weights w_j in Eq.(4). The proposed kernel is expressed as a spline, which can theoretically approximate any continuous function. Furthermore, by considering the cylindrical geometry of the underlying fibers in the tissue [25] the spline model can be reduced to a 2-dimensional spline over the 2D domain $b \times |\mathbf{g} \cdot \mathbf{v}_j|$ as follows:

$$K(b, \mathbf{g}|\mathbf{v}_j) = \sum_k \sum_l c_{k,l}\psi_l(b)\psi_k(|\mathbf{g} \cdot \mathbf{v}_j|) \tag{5}$$

where $c_{k,l}$ are the so-called unknown control points, and $\psi_i(x)$ is a spline basis. In the special case of HARDI acquisition using a constant b-value, the formula for the corresponding adaptively shaped kernel is simplified to an 1-dimensional spline given by

$$K(\mathbf{g}|b, \mathbf{v}_j) = \sum_k c_k\psi_k(|\mathbf{g} \cdot \mathbf{v}_j|). \tag{6}$$

Figure 1 illustrates the 2D and 1D splines that correspond to Eq.(5) and Eq.(6) respectively computed from simulated DW-MRI data. As expected, the diffusion-weighted MR signal attenuation S/S_0 decreases while b-value increases and also decreases when the magnetic gradient direction $\mathbf{g}$ becomes parallel to the fiber orientation $\mathbf{v}$.

By substituting Eq.6 into Eq.4 we derive our model which is given by Eq.(7).

$$S(\mathbf{g})/S_0 = \sum_{j=1}^{N} w_j \sum_k c_k\psi_k(|\mathbf{g} \cdot \mathbf{v}_j|) \tag{7}$$

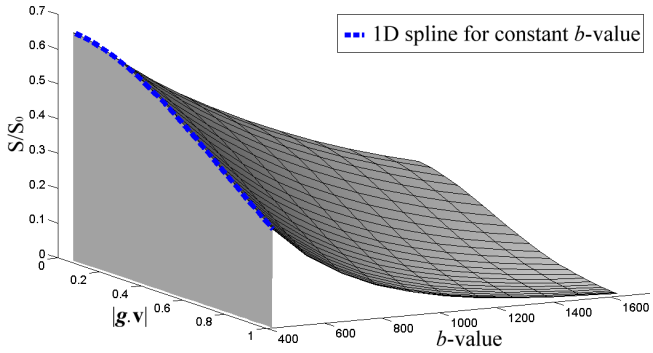

Fig. 1. Plot of the 2D spline that corresponds to $K(b, \mathbf{g}|\mathbf{v})$ computed from simulated DW-MRI data of a single fiber with orientation $\mathbf{v}$. The dashed line is a plot of the 1D spline that corresponds to $K(\mathbf{g}|b, \mathbf{v})$ for a constant b-value using the same simulated dataset.

The unknowns in this model are the weights w_j and the control points c_k. The number of the unknown weights w_j corresponds to the resolution of the hemisphere tessellation by the vectors $\mathbf{v}_j$, and the number of the control points c_k corresponds to the resolution of the discretization of the spline. Here we should emphasize that the adaptively shaped kernel employed in Eq. 7 can theoretically approximate any kernel function and therefore it does not add any kind of limitation related to the underlying fiber characteristics, which is one of the major advantages of our model when compared with the existing techniques. In the next section we estimate these unknowns from a given DW-MRI dataset.

3 Algorithm and implementation details

In this section we assume that a set of M diffusion-weighted MRI images S_i are given, along with the corresponding magnetic gradient directions $\mathbf{g}_i$. The underlying fiber populations in this dataset can be reconstructed by using our adaptively-shaped kernel model (Eq.7) in a least-square minimization framework, by minimizing the following objective function

$$E(\mathbf{w}, \mathbf{c}) = \sum_{i=1}^{M} \left(S_i/S_0 - \sum_{j=1}^{N} w_j \sum_{k=1}^{P} c_k \psi_k(|\mathbf{g}_i \cdot \mathbf{v}_j|) \right)^2 \tag{8}$$

where $\mathbf{w}$ and $\mathbf{c}$ are the two unknown vectors that consist of the unknown variables w_j and c_k.

Any spline basis function can be used for $\psi_k(x)$ in Eq.8. In our experiments we employed the B-spline basis of various orders due to their simple analytic form, and the corresponding control points were positioned on a uniform grid of knots. The number of control points P controls the flexibility of the estimated

adaptive kernel, i.e. large P can accommodate more bumps in the approximated kernel function. However, in our particular application the kernel function should represent the diffusion-weighted MRI signal attenuation of a single fiber, which is a very smooth function (see Fig.1) and therefore can be well approximated by using a small number of control points ($P \sim 5$).

Additionally, the diffusion-weighted MRI signal attenuation of a single fiber is a monotonically decreasing function of $|\mathbf{g}_i \cdot \mathbf{v}_j|$, (or monotonically increasing function of $1 - |\mathbf{g}_i \cdot \mathbf{v}_j|$) due to the physics of DW-MRI acquisition. Hence the corresponding adaptively-shaped kernel should also be a monotonically increasing function of $1 - |\mathbf{g}_i \cdot \mathbf{v}_j|$, which can be incorporated into our parametrization by enforcing the corresponding unknown control points c_k to form a monotonically increasing sequence. This can be achieved by further parameterizing the sequence of control points as: $c_1 = a_1$, $c_2 = a_1 + a_2$,..., $c_k = \sum_{l=1}^{l=k} a_l$ where $a_1, \ldots, a_k$ is a sequence of non-negative numbers. By plugging the parameters a_k into Eq.8 we arrive at the following expression for the objective function

$$E(\mathbf{w}, \mathbf{a}) = \sum_{i=1}^{M} \left(S_i/S_0 - \sum_{j=1}^{N} w_j \sum_{k=1}^{P} a_k \sum_{l=k}^{P} \psi_l (1 - |\mathbf{g}_i \cdot \mathbf{v}_j|) \right)^2 \tag{9}$$

where $\mathbf{a}$ is the unknown vector that consists of the parameters a_k. This minimization problem can be solved iteratively by first estimating $\mathbf{w}$ given $\mathbf{a}$ and then estimating $\mathbf{a}$ given $\mathbf{w}$. Note that all the unknown parameters should be non-negative real numbers and therefore they can be computed using the non-negative least squares method [26].

Both vectors $\mathbf{w}$ and $\mathbf{a}$ can be estimated by solving two linear systems. First we form the linear system $\mathbf{A}\mathbf{w} = \mathbf{b}$, where the matrix $\mathbf{A}$ is of size $M \times N$, and its elements are $A_{i,j} = \sum_{k=1}^{P} a_k \sum_{l=k}^{P} \psi_l (1 - |\mathbf{g}_i \cdot \mathbf{v}_j|)$ and the elements of $\mathbf{b}$ are $b_i = S_i/S_0$. After having solved this linear system using non-negative least squares, we form another linear system $\mathbf{A}'\mathbf{a} = \mathbf{b}$, where the matrix $\mathbf{A}'$ is of size $M \times P$, and its elements are $A'_{i,k} = \sum_{j=1}^{N} w_j \sum_{l=k}^{P} \psi_l (1 - |\mathbf{g}_i \cdot \mathbf{v}_j|)$. This system should also be solved using a non-negative least squares approach. These two alternating steps are repeated until convergence of the algorithm. The convergence of the algorithm is guaranteed, due to the fact that both steps converge and reduce the same positive-valued objective function (Eq. 9).

The process for reconstructing fibers using adaptively-shaped kernels is summarized in Algorithm 1. As was previously discussed, *argmin* is implemented by solving a linear system using the non-negative least squares method. In order to increase the robustness of the adaptively-shaped kernel method to the presence of noise in the data, we can slightly modify our algorithm by penalizing the smallest weights from vector $\mathbf{w}$ when updating the vector $\mathbf{a}$. The dominant weights correspond to strong fiber responses, while the smallest weights capture high frequency details such as noise. In our experiments, in the step for updating vector $\mathbf{a}$, we employed a penalizing function that scales down by a factor 0.5 those weights w_j that have less than half of the strength of the largest weight in $\mathbf{w}$. Other penalizing functions can be employed as well.

input : $S_1 \dots S_M$, $\mathbf{g}_1 \dots \mathbf{g}_M$, S_0, b-value, and a small tolerance value e
output: the vector of weights $\mathbf{w}$ and the vector of control points $\mathbf{c}$
$t \leftarrow 0$;
while $\| a_t - a_{t-1} \| > e$ **do**
  $\mathbf{w} \leftarrow argmin_{\mathbf{w}} E(\mathbf{w}, \mathbf{a})$ given $\mathbf{a}$;
  $\mathbf{a} \leftarrow argmin_{\mathbf{a}} E(\mathbf{w}, \mathbf{a})$ given $\mathbf{w}$;
end
for $k = 1 \dots P$ **do**
  $c_k \leftarrow \sum_{l=1}^{l=k} a_l$;
end

Algorithm 1: Adaptively-shaped kernels for multi-fiber reconstruction

Finally, after having approximated the DW-MRI signal by using the proposed adaptively-shaped kernel model, we can estimate the fiber orientations by finding the maxima of the water molecule displacement probability given by the Fourier integral

$$P(\mathbf{r}) = \int \frac{S(\mathbf{q})}{S_0} e^{-2\pi i \mathbf{q}^T \mathbf{r}} d\mathbf{q} \tag{10}$$

where $\mathbf{q}$ is the reciprocal space vector, $S(\mathbf{q})/S_0$ is the approximated DW-MRI signal value associated with vector $\mathbf{q}$, and $\mathbf{r}$ is the displacement vector. Note that vector $\mathbf{q}$ is a function of the b-value and the magnetic gradient direction $\mathbf{g}$. However, if the adaptively-shaped kernel model is fitted to data that were acquired using a constant b-value, then the estimated kernel is given by Eq.6, which is not a function of b-value. In this case the fiber orientations can be computed by finding the maxima of the following approximated expression

$$P(\mathbf{r}) \simeq \sum_{j=1}^{N} w_j \sum_{k=1}^{P} c_k \int \psi_k(|\mathbf{g} \cdot \mathbf{v}_j|) e^{-2\pi i \|\mathbf{q}\| \mathbf{g}^T \mathbf{r}} d\mathbf{g} \tag{11}$$

where the integrals $\int \psi_k(|\mathbf{g} \cdot \mathbf{v}_j|) e^{-2\pi i \|\mathbf{q}\| \mathbf{g}^T \mathbf{r}} d\mathbf{g}$ form a new basis that can be precomputed numerically over a set of predefined displacement vectors $\mathbf{r}$.

In the next section we demonstrate the results of application of our algorithm to synthetic and real DW-MRI datasets.

4 Experimental results

This section is divided into two subsections: a) Synthetic data experiments and b) experiments using real DW-MRI data from excised rat hippocampus and optic chiasm.

4.1 Synthetic data experiments

The data employed in the experiments of this section were synthesized using the realistic simulation model proposed in [25]. This method simulates the DW-MRI

signal attenuation from water molecules, whose diffusion is restricted inside a cylindrical fiber of radius ρ and length L. We employed this model to simulate a 2-fiber crossing (depicted in Fig. 2 left) using the parameters $\rho = 5\mu m$, $L = 5mm$, b-value $= 1500s/mm^2$ which are typical values in rat brain datasets [8]. The dataset were simulated using 81 gradient directions computed as the 3rd-order tessellation of the icosahedron on the unit hemisphere.

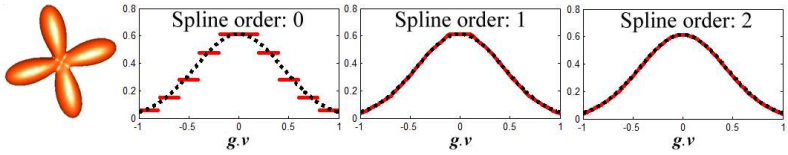

Fig. 2. Plots of the kernels computed by applying our algorithm to a synthetic dataset from a 2-fiber crossing (left) using various orders of the spline basis. The dotted line is the ground truth (simulated signal from a single fiber).

First, in order to demonstrate the ability of our algorithm in estimating an accurate deconvolution kernel (i.e. single fiber response) from a 2-fiber crossing, we applied it to the simulated dataset using various orders of the b-spline basis $\psi_k(x)$ used in the kernel parametrization. By observing the recovered kernels (Fig. 2), we can see that for each order of the B-spline used, the recovered kernel was the closest possible approximation of the simulated signal from a single fiber (dotted line). In the 2^{nd}-order case there was perfect match with the ground truth (floating precision degree error). Here we should emphasize that neither the number of fibers nor the shape of the deconvolution kernel (single fiber response) were known in our algorithm. This is in contrast to the existing methods, which employ a given fixed deconvolution kernel. The estimated control points c_k for order-2 are shown in Fig. 3.

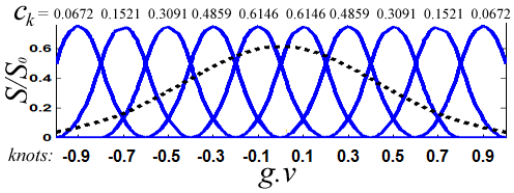

Fig. 3. The control points c_k computed by applying our algorithm to the simulated dataset. The plots of the b-spline basis are shown along with the evaluated kernel (dotted line). The centers of the basis (knots) are also marked.

In the next experiment, we added various levels of Riccian noise to the simulated 2-fiber crossing dataset and then tested the accuracy of several competing

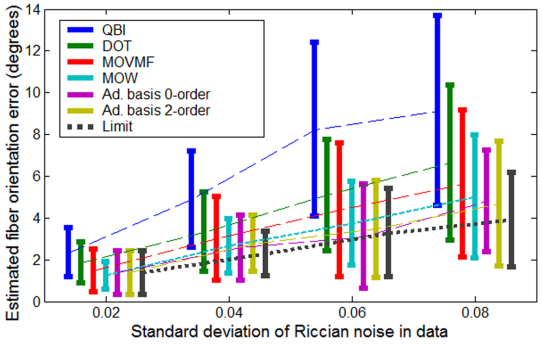

Table of errors (in degrees)
noise st. dev.=0.08

Method	Mean	St. dev.
QBI	9.125	± 4.545
DOT	6.645	± 3.720
MOVMF	5.624	± 3.514
MOW	5.010	± 2.955
Ad.bas-0	4.791	± 2.425
Ad.bas-2	4.669	± 2.985
Limit	3.898	± 2.258

Fig. 4. Comparison of the estimated fiber orientation errors produced by several multi-fiber reconstruction models (QBI [11], DOT [8], MOVMF [22], MOW [20], and our adaptive kernel technique) using simulated 2-fiber crossing data.

multi-fiber reconstruction techniques in estimating fiber orientations. The fiber orientations were estimated by finding the maxima of either the displacement probability or the ODF computed by the corresponding methods. We used four distinct noise levels and for each noise level the experiments were repeated 100 times. The obtained results are shown in Fig. 4 and for the particular noise level with std. dev.= 0.08 the errors are reported in the table. The results demonstrate the superiority of the proposed model. Furthermore, there was no significant difference between the results obtained by the 0^{th} and the 2^{nd}-order B-spline basis, both of which yielded more accurate results compared to the other methods.

The last entry in the table in Fig. 4 corresponds to results obtained using the simulated single fiber response as the deconvolution kernel K in the spherical deconvolution framework (Eq. 4). Since this kernel is identical to the simulated single fiber response used in data generation, we will consider the multi-fiber reconstruction results produced by using it as the limiting case, which corresponds to the theoretic best possible result. Note that our method is the only method that produces average errors smaller than 1 degree compared to the limiting case. Finally we can further improve the results produced by all the methods by using post-processing tools such as ODF sharpening similar to that presented in [14], however in our experiments we compared the strength of each individual model without using any additional post-processing supplements.

4.2 Real data experiments

In this section we present experimental results obtained using real data set from excised rat hippocampus (shown in Fig. 5) and optic chiasm (shown in Fig. 6). The original DW-MRI data sets contained 22 images acquired using a pulsed gradient spin echo pulse sequence, with 21 different diffusion gradients and approximate b value of 1250 s/mm^2.

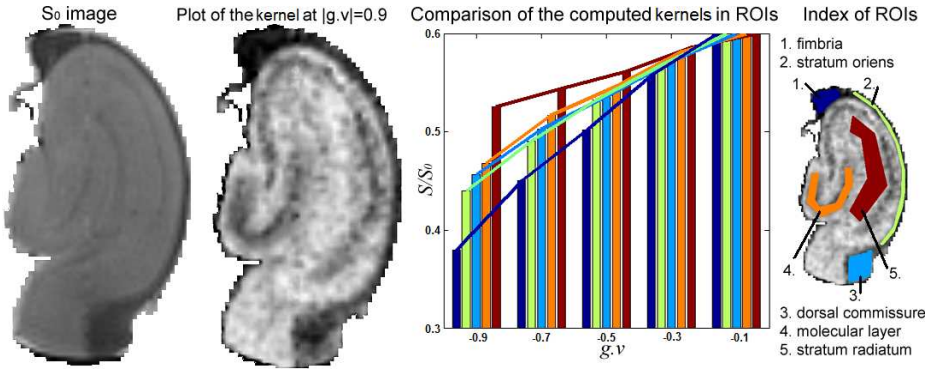

Fig. 5. The adaptively-shaped kernels estimated from a hippocampal DW-MRI dataset. The S_0 image is shown on the left and then the estimated kernel (Eq. 6) evaluated at $|\mathbf{g} \cdot \mathbf{v}| = 0.9$. The plot of the average adaptive kernel in various ROIs is shown as a bar chart on the right.

We applied the proposed method to the hippocampal dataset using 2^{nd}-order b-spline and 5 control points c_k. In order to demonstrate the variability of the shape of the estimated deconvolution kernel across the dataset, we depict the estimated kernel (eq. 6) evaluated at $|\mathbf{g} \cdot \mathbf{v}| = 0.9$ as an image in Fig. 5b. As we expected, the regions of high anisotropy appear darker, since the signal is more attenuated in such regions when the gradient direction $\mathbf{g}$ forms a small angle with the fiber orientation $\mathbf{v}$. This demonstrates that our method estimates clinically meaningful deconvolution kernels, which vary across the field, contrary to the existing methods, which employ a pre-defined fix-shaped kernel.

Furthermore, the plot in Fig 5 shows the average adaptively-shaped kernel estimated in various regions of interest (ROI) in hippocampus. By observing the plot we can see that fimbria contains more anisotropic fibers, which corresponds to steeper kernel shape, while stratum radiatum contains less anisotropic fibers, which corresponds to flattened kernel shape. These results are validated by the existing knowledge on hippocampal anatomy [27]. This motivates the use of our method, which is based on the cylindrical geometry of fibers as well as the physics of the DW-MRI acquisition, unlike othe existing techniques that require the cylindrical geometry assumption but with prespecified dimensions of the cylinder (not required in our case).

Finally, in Fig. 6 we present multi-fiber reconstruction results from a DW-MRI dataset of an excised rat's optic chiasm. The spherical function plots depict the estimated displacement probability profiles (Eq. 11) at each lattice point. The region of interest is marked with a box in the S_0 image. The depicted field contains spherical plots that correspond to single fibers as well as fiber crossings and other complex probability profiles.

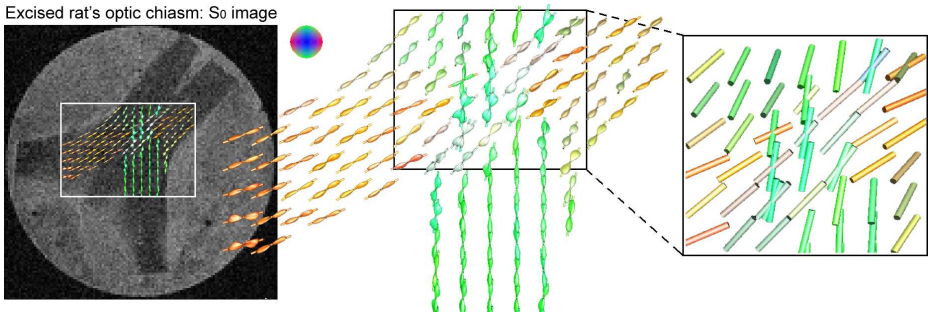

Fig. 6. The field of displacement probabilities estimated by the proposed technique using data from an excised rat's optic chiasm.

5 Conclusions

In this paper, we presented an algorithm that uses adaptively-shaped kernels for multi-fiber reconstruction. In this algorithm, we simultaneously estimate the shape of the kernel with the rest of the unknown parameters in the model. Our technique is motivated by the fact that the characteristics of the underlying fibers vary across a dataset, which corresponds to variations in the shape of the deconvolution kernel. The method was tested on synthetic and real DW-MRI datasets. The experimental results demonstrate the superiority of our model over existing techniques. We validated our algorithm by presenting quantitative as well as visual results. Our future efforts will be focused on employing the proposed method in multi-fiber tracking framework in order to study the changes on the shape of the estimated kernels along known fiber bundles in the brain.

References

[1] LeBihan, D., et al: MR imaging of intravoxel incoherent motions: Application to diffusion and perfusion in neurologic disorders. Radiology **161** (1986) 401–407
[2] Basser, P.J., et al: Estimation of the effective self-diffusion tensor from the NMR spin echo. J. Magn. Reson. B **103** (1994) 247–254
[3] Frank, L.: Characterization of anisotropy in high angular resolution diffusion weighted MRI. Magn. Reson. Med. **47**(6) (2002) 1083–1099
[4] Alexander, D.C., et al: Detection and modeling of non-Gaussian apparent diffusion coefficient profiles in human brain. MRM **48**(2) (2002) 331–340
[5] von dem Hagen, E.A.H., Henkelman, R.M.: Orientational diffusion reflects fiber structure within a voxel. Magn. Reson. Med. **48**(3) (2002) 454–459
[6] Tuch, D.S., et al: High angular resolution diffusion imaging reveals intravoxel white matter fiber heterogeneity. MRM **48**(4) (2002) 577–582
[7] Barmpoutis, A., et al: Symmetric positive 4th order tensors and their estimation from diffusion weighted mri. In: IPMI. (2007) 308–319

[8] Özarslan, E., et al: Resolution of complex tissue microarchitecture using the diffusion orientation transform. NeuroImage **36**(3) (July 2006) 1086–1103
[9] Zhan, W., Yang, Y.: How accurately can the diffusion profiles indicate multiple fiber orientations? a study on general fiber crossings in diffusion MRI. Journal of Magnetic Resonance **183**(2) (2006) 193–202
[10] Wedeen, V.J., et al: Mapping complex tissue architecture with diffusion spectrum magnetic resonance imaging. MRM **54**(6) (2005) 1377–1386
[11] Tuch, D.S.: Q-ball imaging. Magn. Reson. Med. **52**(6) (2004) 1358–1372
[12] Anderson, A.W.: Measurement of fiber orientation distributions using high angular resolution diffusion imaging. MRM **54**(5) (2005) 1194–1206
[13] Hess, C.P., et al: Q-ball reconstruction of multimodal fiber orientations using the spherical harmonic basis. MRM **56**(1) (2006) 104–117
[14] Descoteaux, M., Angelino, E., Fitzgibbons, S., Deriche, R.: Regularized, fast and robust analytical q-ball imaging. MRM **58** (2007) 497–510
[15] Behrens, T., et al: Characterization and propagation of uncertainty in diffusion-weighted mr imaging. Magn. Reson. Med. **50**(2) (2003) 1077–1088
[16] Assaf, Y., et al: New modeling and experimental framework to characterize hindered and restricted water diffusion in brain white matter. MRM **52**(5) (2004) 965–978
[17] Hosey, T.P., et al: Inference of multiple fiber orientations in high angular resolution diffusion imaging. MRM **54**(6) (Dec 2005) 1480–1489
[18] Behrens, T., et al: Probabilistic tractography with multiple fibre orientations: What can we gain? NeuroImage **34** (2007) 144–155
[19] Tournier, J.D., Calamante, F., Gadian, D.G., Connelly, A.: Direct estimation of the fiber orientation density function from diffusion-weighted MRI data using spherical deconvolution. NeuroImage **23**(3) (2004) 1176–1185
[20] Jian, B., et al: A novel tensor distribution model for the diffusion weighted MR signal. NeuroImage **37**(1) (2007) 164–176
[21] Ramirez-Manzanares, A., et al: Diffusion basis functions decomposition for estimating white matter intravoxel fiber geometry. IEEE Trans. Med. Imaging **26**(8) (2007) 1091–1102
[22] Kumar, R., et al: Multi-fiber reconstruction from DW-MRI using a continuous mixture of von mises-fisher distributions. In: MMBIA. (2008)
[23] Rathi, Y., Michailovich, O., Bouix, S., Shenton, M.: Directional functions for orientation distribution estimation. In: ISBI (2008) 927–930
[24] Jian, B., Vemuri, B.C.: A unified computational framework for deconvolution to reconstruct multiple fibers from diffusion weighted MRI. IEEE Trans. Med. Imaging **26**(11) (2007) 1464–1471
[25] Söderman, O., Jönsson, B.: Restricted diffusion in cylindirical geometry. J. Magn. Reson. B **117**(1) (1995) 94–97
[26] Lawson, C.L., Hanson, R.J.: Solving Least Squares Problems. Englewood Cliffs, NJ: Prentice-Hall (1974)
[27] Shepherd, T.M., et al: Structural insights from high-resolution diffusion tensor imaging and tractography of the isolated rat hippocampus. NeuroImage **32**(4) (2006) 1499–1509